THE ASTROPHYSICAL JOURNAL, 385:306–313, 1992 January 20

IRAS 16293−2422: A VERY YOUNG BINARY SYSTEM?

LEE G. MUNDY,[1] ALWYN WOOTTEN,[2] BRUCE A. WILKING,[3] GEOFFREY A. BLAKE,[4] AND ANNEILA I. SARGENT[5]
Received 1991 February 14; accepted 1991 July 22

ABSTRACT

We present 4″.5 × 2″.5 resolution millimeter wavelength observations of the young far-infrared source IRAS 16293−2422 which resolve the continuum emission into two sources, MM 1 and MM 2. These sources coincide with known radio continuum sources and may constitute a very young binary system with a projected separation of 840 AU. Flux measurements from 18 cm to 25 μm show that the majority of the millimeter wavelength emission arises from dust within 300 AU of the individual central objects. The total dynamical mass of 1.1–1.3 $M_\odot$, coupled with our mass estimates for MM 1 and MM 2, suggests that the mass in circumstellar material is comparable to that of the central stellar cores. Since the stellar masses are constrained to be $\leq 0.5\ M_\odot$ each, it is likely that the bolometric luminosity of 30–40 $L_\odot$ is derived mainly from accretion of the observed circumstellar material.

Maps of the $J = 2, 3–1, 2$ transition of SO obtained simultaneously show that this emission is centered on MM 1, with weaker emission in a clumpy distribution to the east and west. No SO emission is detected toward MM 2, indicating an upper limit to the fractional abundance which is a factor of 10 below that toward MM 1. We propose that the SO emission toward MM 1 is a result of the outflow activity associated with this source and that the outlying emission clumps trace regions of mild interaction between the outflow and the ambient cloud.

Subject headings: circumstellar matter — infrared: stars — stars: individual (IRAS 16293−2422) — stars: pre–main-sequence

1. INTRODUCTION

Near-infrared imaging of stellar populations within molecular clouds indicates that it is rare for stars to form in isolation. For example, in the Orion giant molecular cloud, high spatial resolution, deep images with infrared array cameras show that the majority of stars are forming in clusters (e.g., Lada et al. 1991; McCaughrean et al. 1991). These findings emphasize the long-standing problem of source confusion in the 30″ or larger beams traditionally used to study young stellar objects at far-infrared and millimeter wavelengths. Indeed, considering the properties of optically identified binary and multiple star systems, any statement that an observation includes a single forming star within even a 5″ beam must be viewed with caution on a purely statistical basis. For example, recent studies of both B2–B5 stars and F7–G9 stars find that about 75% of all stars are in multiple star systems (Abt, Gomez, & Levy 1990; Duquennoy & Mayor 1990).

In light of this gregarious nature of stars, it should not be surprising that the number of candidate binary and multiple star systems among young stellar objects is growing as these objects are studied with higher resolution and sensitivity. For example, 2 μm lunar occultation observations of young stellar objects (YSOs) in Taurus and Ophiuchus have revealed that nine of 31 (29%) are binaries with separations of 0″.01–0″.63 (Simon et al. 1987; Chen et al. 1990). Near-infrared speckle interferometry and array camera imaging have also revealed companions of both pre–main-sequence and deep embedded YSOs with projected separations greater than 0″.15 and 1″, respectively (e.g., Chelli et al. 1988; Zinnecker, Perrier, & Chelli 1988; Rieke, Ashok, and Boyle 1989; Barsony et al. 1989). These young and forming binary systems can provide important clues to the nature and origin of multiple star systems. Among the key issues to be addressed are the questions of coeval formation versus capture theories and core fission/fragmentation versus independent core origins.

This paper presents very high spatial resolution millimeter and centimeter wavelength observations of a proposed proto–binary system in the nearby (160 pc) Ophiuchus molecular complex. IRAS 16293−2422 is a cold but intense far-infrared and millimeter-wave source, radiating only 30–40 $L_\odot$ (Walker et al. 1986; Mundy, Wilking, & Myers 1986; Walker, Adams, & Lada 1990). This deeply embedded source is also associated with a complex molecular outflow and a group of H_2O masers (Wootten & Loren 1987; Walker et al. 1988; Mizuno et al. 1990; Wilking & Claussen 1987; Wootten 1989). Previous interferometric millimeter wavelength observations with a resolution of 6″.3 × 4″.5 have shown coextensive dust continuum and molecular emission arising from a 11″ × <5″ region around IRAS 16293−2422. This molecular emission exhibits a velocity gradient suggestive of a circumstellar disk (Mundy, Wootten, & Wilking 1990). However, the presence of two discrete radio sources with a projected separation of 5″ lying within the elongated millimeter emission region raises the possibility that the extension is due to the presence of two unresolved objects rather than a circumstellar disk (Wootten 1989). We have undertaken higher resolution millimeter and centimeter wavelength continuum observations to study

[1] Astronomy Program, University of Maryland, College Park, MD 20742.
[2] National Radio Astronomy Observatory, Edgemont Road, Charlottesville, VA 22903-2475.
[3] Harvard-Smithsonian Center for Astrophysics; and Department of Physics & Astronomy, University of Missouri-St. Louis, 8001 Natural Bridge Road, St. Louis, MO 63121.
[4] Division of Geological and Planetary Sciences, California Institute of Technology, Pasadena, CA 91125.
[5] Owens Valley Radio Observatory, California Institute of Technology. Postal address: Downes Laboratory of Physics 320-47, California Institute of Technology, Pasadena, CA 91125.

further this unusual source and, in particular, to determine if it is a binary system.

2. OBSERVATIONS

2.1. *Millimeter Wavelength Data*

Aperture synthesis mapping of the SO J, $K = 2, 3–1, 2$ transition at 109.2522 GHz and the $\lambda = 2.75$ mm continuum toward IRAS 16293−2422 [$\alpha(1950) = 16^h29^m20^s.9$, $\delta(1950) = -24°22'13''.0$] was carried out with the three-element Owens Valley Radio Observatory Millimeter Wavelength Interferometer during the period 1988 April to 1989 March. The correlator consisted of 32 1 MHz channels, 32 50 kHz channels, and a 300 MHz broad-band channel. The 1 MHz filters give a total velocity coverage of 88 km s^{-1}. To provide extended velocity coverage at 50 kHz resolution, the source was observed in two velocity settings separated by 2.75 km s^{-1}, giving a total velocity coverage of 7.1 km s^{-1} centered on 4.0 km s^{-1}. Data were acquired in eight configurations with baselines out to 140 m north-south and 200 m east-west yielding a synthesized beam of $4''.5 \times 2''.5$ with position angle of 13°.6. NRAO 530 was observed at 30–40 minute intervals as a phase calibrator and secondary flux standard. Mars ($T_B = 207$ K) and Uranus ($T_B = 130$ K) were the primary flux calibrators. The absolute uncertainties in positions and fluxes are approximately 0.15 of the synthesized beam (0".6) and 20%, respectively.

Maps were made using the CLEAN algorithm in AIPS. Because the receivers were tuned to have nearly single-sideband response during the majority of the observations, the continuum maps were made only for the lower sideband. Although also present in this sideband, the SO line emission, averaged over the continuum channel bandwidth, contributes at most 10 mJy beam^{-1}, a value comparable to the rms noise in the continuum map of 9 mJy beam^{-1}. Continuum emission was removed from the line channel maps by subtracting the continuum map scaled by the ratio of the channel width to continuum bandwidth. The rms noise levels in the final 1 MHz and 200 kHz (sums of four 50 kHz channels) maps were 80 and 180 mJy beam^{-1}, respectively.

2.2. *Centimeter Wavelength Data*

The "A" configuration of the Very Large Array[6] (VLA) was used to observe IRAS 16293-2422 at frequencies centered at 22.46 GHz ($\lambda = 1.3$ cm) and 8.44 GHz ($\lambda = 3.6$ cm) with a 100 MHz bandwidth on 1989 January 20. Observations were also made in the "A" array at the frequencies of the 1.665 and 1.667 GHz OH lines, with a channel width of 3 kHz (0.55 km s^{-1}) and a total bandwidth of 195 kHz. On-source integration time at each frequency was roughly 40 minutes. The flux scales for the data were based on observations of 3C 286 adopting fluxes of 2.55, 5.18, and 13.74 Jy at 22.46, 8.44, and 1.67 GHz, respectively. The phase calibrator was 1622−297, for which the derived fluxes are 1.77, 1.85, and 2.78 Jy at the above frequencies. Natural weighting maps at 22.46 and 1.67 GHz provided resolutions of $0''.18 \times 0''.085$ and $1''.0 \times 1''.0$, respectively, and RMS noise levels of 130 and 1300 μJy. The uniform weighting map at 8.44 GHz had a resolution of $0''.34 \times 0''.17$ and an RMS noise level of 30 μJy.

3. RESULTS

3.1. *Continuum Observations*

Millimeter wavelength continuum and integrated SO line emission maps of the IRAS 16293−2422 region are shown in Figure 1. The continuum emission clearly arises from two sources, MM 1 (southeast) and MM 2 (northwest), which are spatially coincident with the centimeter wavelength emission regions A1–A2 (MM 1) and B (MM 2) mapped by Wootten 1989). Results of a Gaussian fit to each peak are given in Table 1. MM 1 is marginally resolved with a formal fitted size of $4''.3 \times 3''.0$ ($\pm 0''.3$) at position angle 165°; MM 2 is unresolved, $\leq 2''.5$ in diameter. Given the sparse sampling at high spatial frequencies, and the uncertainties associated with the combination of data over multiple configurations, we can not rule out the possibility that MM 1 is also unresolved.

[6] The National Radio Astronomy Observatory is operated by Associated Universities, Inc., under cooperative agreement AST-8814514 with the National Science Foundation.

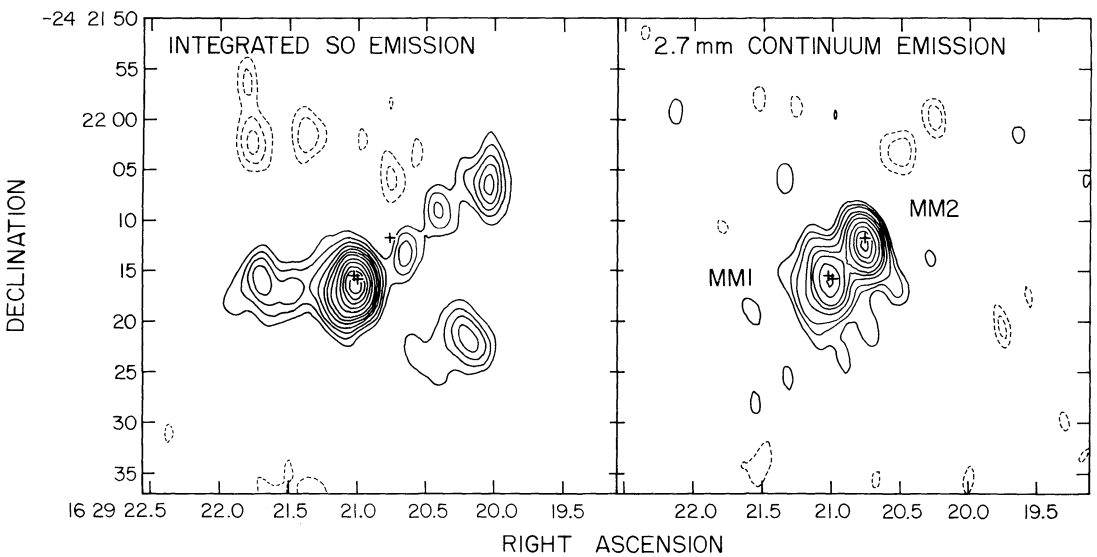

FIG. 1.—Integrated SO $J = 2, 3–2, 1$ line emission (left) and 2.75 mm continuum emission (right) from IRAS 16293−2422. The contours for the line map are −4, −3, −2, 2, 3, 4, 5, 6, 7, 8, 9, 10, 12, 14, 16, and 18 times 0.37 Jy beam^{-1} km s^{-1}. The contours for the continuum map are −4, −2, 2, 4, 6, 8, 10, 12, 14, 18, 22, 26, and 30 times 7.5 mJy beam^{-1}. The beam for both maps was $4''.5 \times 2''.5$ with a position angle of 13°.6. The plus signs mark the positions of the centimeter wavelength emission sources (Wootten 1989; this work). Coordinates are epoch 1950.

TABLE 1

RESULTS OF $\lambda = 2.75$ MILLIMETER OBSERVATIONS

Property	MM 1	MM 2
R.A. (1950)	$16^h29^m21^s.05$	$16^h29^m20^s.77$
Decl. (1950)	$-24°22'15''.9$	$-24°22'12''.4$
Peak continuum flux (mJy beam^{-1})	146	235
Integrated continuum flux (mJy)[a]	350	260
Continuum source size[a]	$4''.3 \times 3''.0$	$\leq 2''.5$
Peak SO line flux (Jy beam^{-1})	1.1	<0.25[b]
Velocity-integrated SO line flux (Jy beam^{-1} km s^{-1})	7.2	<1.1[b]
Line source size	$4''.0 \times 2''.4$	...

[a] Results from Gaussian fit.
[b] 3 σ upper limit.

The total continuum flux and source positions derived here are consistent with previous millimeter wavelength observations at lower resolution (Mundy et al. 1986; Mundy et al. 1990). In fact, constrained Gaussian fits to the lower resolution data by Wootten (1989) yield fluxes for the individual sources similar to those in Table 1. Effectively, all of the flux in previous millimeter interferometer maps can be accounted for by MM 1 and MM 2 in the current maps.

Two primary emission regions are also present in the continuum maps at 22.5 and 8.4 GHz as shown in Figure 2. No emission was detected from either the OH lines or continuum at 1.67 GHz. As previously seen at 15 GHz (Wootten 1989), source A breaks up into two main components, A1 (east) and A2 (west), with perhaps two additional weak components visible in the 22.5 GHz map. Source B is marginally resolved at 22.5 GHz with a size of $0''.24 \times 0''.17$ (38 AU $\times$ 27 AU at a distance of 160 pc). Positions and fluxes are given in Table 2, along with earlier measurements at 5 and 15 GHz (Wootten 1989). The fluxes are somewhat lower than those given by Estalella et al. (1991) but this difference is probably due to the loss of large-scale flux in our "A" array observations.

Least-squares power-law fits to the 5–22.5 GHz fluxes of sources A and B yield spectral indices of 0.4 ± 0.1 and 2.1 ± 0.4, respectively, which are consistent with the results of Estalella et al. (1991). The flux densities for source A2 are consistently lower than for A1 so that the combined spectral index is dominated by A1; the signal-to-noise ratio does not warrant an independent fit to the emission from A2. As noted by Wootten (1989), the spectral index for A is consistent with emission from a fully ionized wind; the presence of H_2O masers and the larger scale CO outflow also suggests a stellar wind exists. Source B's spectral index is consistent with an optically thick H II region, although the source of ionization remains enigmatic; there are no signs of small-scale outflow activity in this low-luminosity object.

For MM 1/source A, an extrapolation of the 5–22.5 GHz flux densities using the power-law fit yields only a small fraction of the observed 2.75 mm flux. Likewise, an extrapolation of the millimeter flux to centimeter wavelengths using a ν^3–ν^4 law, characteristic of optically thin dust, yields too little flux there, as illustrated in Figure 3*a*. Hence, the emission from this source is best explained as arising from ionized gas at centi-

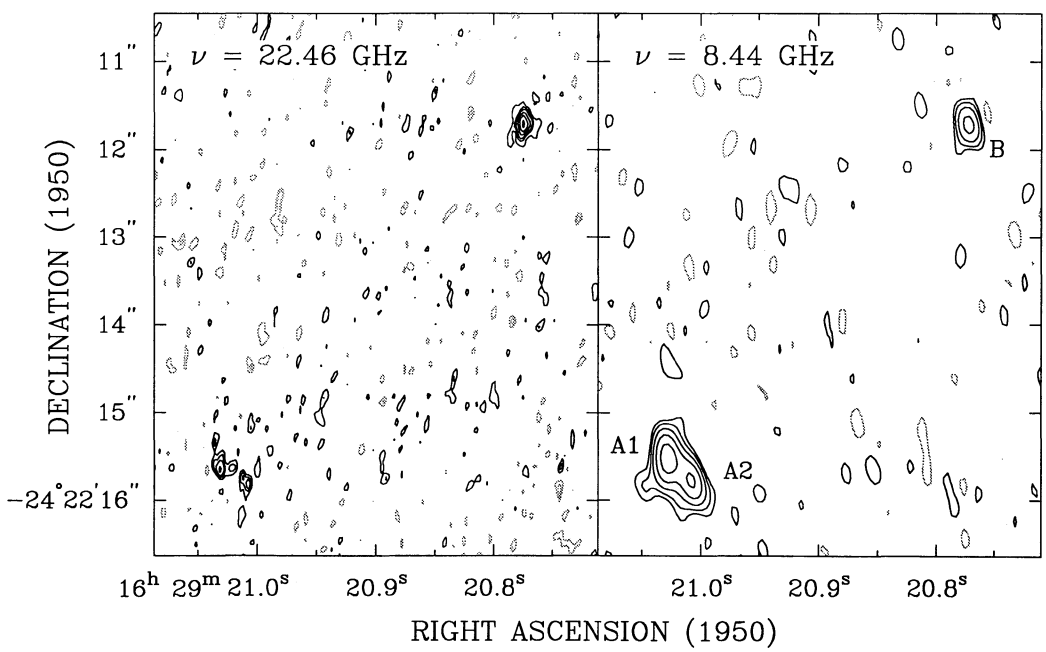

FIG. 2.—Continuum emission at 22.46 GHz (*left*) and 8.44 (*right*) GHz. The 22.5 GHz map was made with natural weighting giving a $0''.18 \times 0''.085$ beam. Contour levels are -3, -2, 2, 3, 4, 6, 8, and 10 times 230 μJy. The 8.4 GHz map was made with uniform weighting giving a $0''.34 \times 0''.17$ beam. Contour levels are -2, 2, 4, 8, 16, 32, and 64 times 30 μJy. The sources are labeled in the right panel.

TABLE 2

RESULTS OF CENTIMETER WAVELENGTH OBSERVATIONS

Property	A1	A2	B
R.A. (1950)	$16^h29^m21^s.029$	$16^h29^m21^s.008$	$16^h29^m20^s.774$
Decl. (1950)	−24°22′15″.57	−24°22′15″.80	−24°22′11″.70
S_ν(22.5 GHz) (mJy)	3.3 ± 0.3	2.0 ± 0.3	7.9 ± 0.8
S_ν(15 GHz) (mJy)[a]	3.5 ± 0.3	1.1 ± 0.3	1.4 ± 0.3
S_ν(8.4 GHz) (mJy)	2.2 ± 0.1	1.6 ± 0.1	0.7 ± 0.07
S_ν(5 GHz) (mJy)[a]	2.7 ± 0.2[b]	...	0.25 ± 0.03
S_ν(1.67 GHz) (mJy)	<1.3	<1.3	<1.3
Deconvolved source size	0″.26 × 0″.11[c]	0″.27 × <0″.10[c]	0″.24 × 0″.17[d]

[a] Fluxes from Wootten 1989.
[b] Sources A1 and A2 unresolved in data; value is total flux.
[c] Fits to 8.4 GHz data; possibility of multiple components.
[d] Fit to 22.5 GHz data; source is marginally resolved.

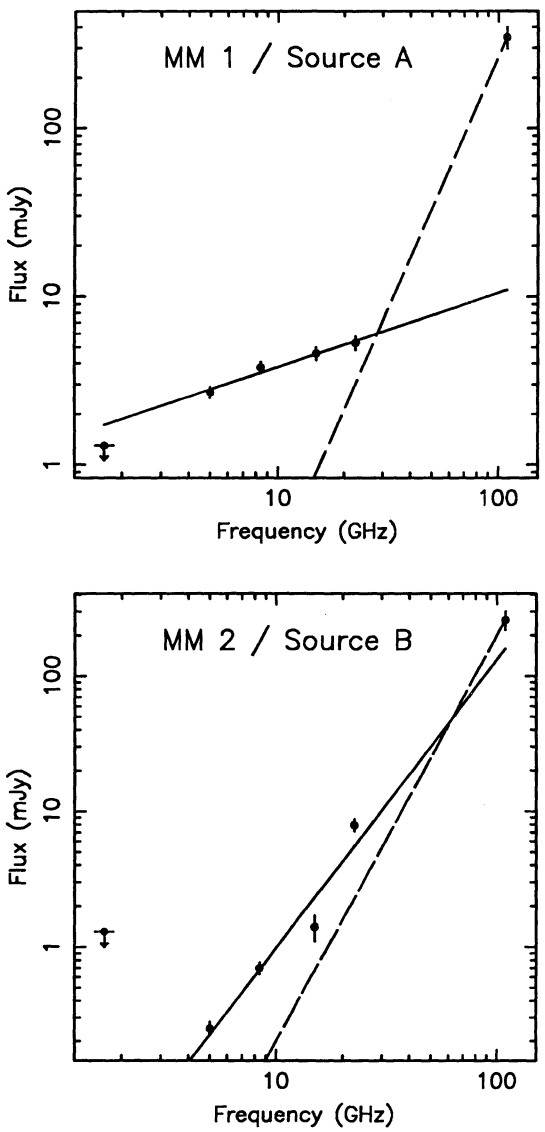

FIG. 3.—Continuum flux measurements for MM 1/source A (*top*) and MM 2/source B (*bottom*). The points with error bars show observed fluxes; downward arrows indicate upper limits. The solid lines show the fits to the centimeter wavelength points and the extrapolation of those fits to 2.75 mm. The long-dashed lines show the extrapolation of the 2.75 mm flux to centimeter wavelengths using $F_\nu \propto \nu^3$.

meter wavelengths and thermal dust at millimeter through mid-infrared wavelengths.

For MM 2/source B, a spectral index of 2.3 ± 0.2 provides a reasonable fit to the continuum data from 5 to 109 GHz (see Fig. 3*b*) raising the possibilities that all of the flux arises from optically thick ionized gas or, perhaps, that source B is not a young stellar object within the Ophiuchus cloud. Considering the latter possibility, it is unlikely that source B is a background Galactic source since Ophiuchus is situated well above the plane of the Galaxy ($b \sim 17°$). It is also not likely to be extra-galactic because such sources rarely have positive spectral indices. Deep 5 GHz surveys by Fomalont et al. (1984) and Maslowski et al. (1984) found that only 5% and 3%, respectively, of the sources in their samples have spectral indices greater than 0.5 and none were greater than 1.1 between 1.4 and 5 GHz. Likewise, 3 mm observations of strong extragalactic radio continuum sources by Edelson (1987) found no sources with spectral indices greater than 0.6 between 20 and 98 GHz. At the same time, it would be unusual for a low-luminosity young stellar object to have an H II region which is optically thick at $\lambda = 2.75$ mm. A survey of 75 ultra compact H II regions by Wood & Churchwell (1989) found that almost all were optically thin at 2 cm; the steepest sources showed spectral indices less than 1 between 15 and 23 GHz. Thus, it is likely that millimeter emission from MM 2 also arises mainly from cool dust while the centimeter emission arises mainly from ionized gas.

An alternative possibility is that the centimeter wavelenth flux from MM 2/source B arises from warm dust in a disk close to the central source. This possibility has been suggested by Estalella et al. (1991) based on lower resolution centimeter wavelength data. Large column densities are required if the observed centimeter wavelength spectral index is produced by dust; $\tau(22.5\ \mathrm{GHz}) = 1$ corresponds to 2×10^{26} H_2 cm^{-2} (0.9 kg cm^{-2}), assuming a λ^{-1} emissivity law. Such a disk would radiate as a blackbody over the peak of its spectral energy distribution. The observed source luminosity of 30–40 $L_\odot$ and 38 × 27 AU source size at 22.5 GHz tightly constrain such disk models. For example, the luminosity of a spatially thin, uniform temperature disk is $L = 33(R/20\ \mathrm{AU})^2(T/250)^4\ L_\odot$. Given the observed peak brightness temperature of 380 K at 22.5 GHz, this simple model fails in that it produces too much luminosity (110 $L_\odot$ for $R = 20$ AU) or too small of source size (9 AU radius for $L = 35\ L_\odot$). Consideration of surface density and temperature gradients in the disk may help in fitting the centimeter wavelength observations; further evaluation of such

disk models is needed. Nevertheless, it is clear that a large disk mass is required if the 8.4–22.5 GHz fluxes arise from optically thick dust. For the uniform temperature disk model, the mass would be $0.35(R/20\ \mathrm{AU})^2\tau(8.4\ \mathrm{GHz})\ M_\odot$.

Comparisons of combined millimeter and far-infrared wavelength flux densities from MM 1 and MM 2 indicate that cool dust emission dominates at submillimeter through far-infrared wavelengths. Based on the flux at 1.3 mm of 5.3 Jy in an 11″ beam (André et al. 1990) and our total 2.75 mm flux of 0.6 Jy, the spectral slope in this wavelength regime, $F_\nu \propto \nu^{2.9}$, is characteristic of dust emission (Woody et al. 1989; Beckwith et al. 1990). Additionally, the 2.75 mm fluxes are well matched by an extrapolation of the 25–1300 μm spectral energy distribution from cool (20–45 K) dust (e.g., Mezger, Sievers, & Zylka 1990; Wootten 1989). Such dust temperatures are inconsistent with the peak brightness temperatures at 22.5 GHz of 200 and 380 K for sources A and B, respectively. Thus, despite the close spatial coincidence of the centimeter and millimeter wavelength emission, it is clear that the millimeter wavelength emission is mainly cool dust emission. The uncertain point is whether the centimeter wavelength emission is due to ionized gas or warm (400 K) dust.

3.2. SO *Emission*

The left panel of Figure 1 shows the SO line emission integrated over 11 km s^{-1} (four channels in the 1 MHz filters) around the line center velocity of $V_{\mathrm{LSR}} = 4.0$ km s^{-1}. The emission is strongest toward MM 1 with a peak flux of 7.2 Jy beam^{-1} km s^{-1} but is not detected toward MM 2 to an rms noise level of 0.4 Jy beam^{-1} km s^{-1}. This latter result is surprising in light of the previous observations which found $C^{18}O$ $J = 1$–0 emission associated with both MM 1 and MM 2 (Fig. 2; Mundy et al. 1990).

In maps with 200 kHz (0.55 km s^{-1}) resolution, the SO emission toward MM 1 appears spread in velocity from 0.5 to 6.5 km s^{-1}, with a maximum of 1.1 Jy beam^{-1} or 10 K in brightness temperature. Weak emission to the east and west of MM 1, evident in Figure 1*b*, can also be traced in the 200 kHz resolution maps. In the case of the western emission, clumps of gas are observed over $\sim$3 km s^{-1} with the strongest blueshifted by $\sim$1.0 km s^{-1} relative to the ambient cloud. The low-level eastern emission has a velocity width (at zero intensity) of $\sim$4 km s^{-1} with the peak emission redshifted by $\sim$2 km s^{-1} relative to the ambient cloud. A possible connection between these low-velocity SO emission clumps with the larger scale high-velocity ($\Delta V = 40$ km s^{-1}) CO outflow will be discussed in § 6. However, the 1 MHz maps clearly show that there is no detectable SO emission corresponding to the high velocity CO gas observed 6 to 20 km s^{-1} from line center (e.g., Walker et al. 1988).

The main SO emission, 16 Jy km s^{-1}, arises from gas which is spatially coincident with the bulk of the dust emitting at millimeter wavelengths around MM 1. A Gaussian fit to the SO emission yields a source position coincident with the MM 1 position to within the formal errors, and a source size of 4″.0 × 2″.4 at position angle 120°, in reasonable agreement with the continuum data. Thus, it is most likely that this gas is cospatial with the emitting dust.

4. A VERY YOUNG BINARY

The presence of compact millimeter continuum emission, high-velocity molecular material, H_2O masers, compact regions of ionized gas, and strong far-infrared emission clearly identify IRAS 16293−2422 with the early stages of star formation. The current observations provide sufficient resolution to divide the dust emission into two components with a projected separation of 840 AU: MM 1, roughly 600 × 400 AU, and MM 2, $\lesssim$400 AU. The coincidence of these peaks with discrete regions of ionized gas emission and the association of MM 1 with H_2O masers support the suggestion by Wootten (1989) that MM 1 and MM 2 are two distinct sites of star formation which appear to form a wide binary system. In fact, the dust distribution on scales less than 2000 AU appears to be completely concentrated on the individual young stellar objects.

Some of the parameters of the putative binary system can be estimated from the observed millimeter wavelength flux densities. The total mass of gas and dust in circumstellar material can be calculated from the 2.75 mm continuum data assuming a dust temperature, emissivity law, and gas-to-dust ratio. We adopt an empirical relation between the 400 μm dust opacity and hydrogen column density, $N(\mathrm{H_2}) = 6 \times 10^{24}\tau_{400}\ \mathrm{H_2\ cm^{-2}}$ (Hildebrand 1983) and scale to 2.75 mm using a λ^{-1} spectral dependence for the dust emissivity (cf. Woody et al. 1989; Weintraub et al. 1989; Beckwith et al. 1990). This corresponds to assuming a mass opacity coefficient of 17 g cm^{-2} at 400 μm. Previous single-temperature fits to the spectral energy distribution of IRAS 16293−2422 yielded a dust temperature of 40 K (Walker et al. 1986; Mundy et al. 1986). The resulting masses of gas and dust are 0.6 $M_\odot$ for MM 1 and 0.4 $M_\odot$ for MM 2; these values are uncertain by factors of 2–3, mainly due to uncertainties in the emissivity law and mass opacity coefficient. Using the source sizes in Table 1, the spherically averaged densities for the two sources are 1×10^9 cm^{-3} and $\geq 2 \times 10^9$ cm^{-3}, respectively.

Although the individual sources are not well resolved in the present observations, the two dust emission regions are sufficiently compact to argue strongly for disklike distributions of the mass. At a radius of 250 AU from a central object, the infall time scale is only 900 $(M/M_\odot)^{-0.5}$ yr. Thus, the observed material would disappear on a time scale of $\sim$1000 yr, unless stabilized or continuously resupplied. If each source is continuously resupplied, the resulting accretion rate would be $5 \times 10^{-3}(M/M_\odot)\ M_\odot\ \mathrm{yr^{-1}}$. This accretion rate results in a luminosity of 4000 $L_\odot$, compared to 30–40 $L_\odot$ estimated from the observed fluxes (Walker et al. 1986; Mundy et al. 1986; Butner et al. 1992), and rapidly builds an unacceptably large central mass. On the other hand, the material is too diffuse and cold to be stabilized by thermal gas pressure, and for a mass of 0.5 $M_\odot$ inside a radius of 250 AU, magnetic support requires a field strength of $\sim$40 mG, much higher than typical interstellar values (Shu, Adams, & Lizano 1987). Rotation, which is the most practical means to stabilize the circumstellar gas against free fall, results in the formation of a disk. The rotational velocity required, assuming a 0.5 $M_\odot$ central object, is 1.5 $(200/R)^{0.5}$ sin i km s^{-1}, where R is in AU and i is the inclination angle. For $R = 200$ AU, this velocity is bearly consistent with the highest velocity $C^{18}O$ emission (Mundy et al. 1990) and may indicate that the inner disk was not detected in $C^{18}O$.

The dynamical mass of the total system (central objects plus gas and dust) can not reliably be estimated from the $C^{18}O$ velocity gradient since that emission may be confined to the individual objects. However, the NH_3 emission appears to be distributed in a large-scale ring around both objects (Mundy et al. 1990) and thus should probe the binary gravitational potential. The full velocity extent of the NH_3 emission in new, higher velocity resolution data (Wootten 1992) is 0.9 km s^{-1} and the

spatial extent is 9000 AU, suggesting an included mass of roughly 1.1/sin i $M_\odot$. Three lines of evidence constrain the inclination angle of the system to be fairly large. First, the outflow appears to be quadrapolar suggesting that we are seeing mostly motion transverse to the outflow axis which is oriented in the plane of the sky (e.g., Cabrit & Bertout 1986). Second, the NH_3 emission "ring" has an axis ratio on the plane of the sky of $\sim$4:1 suggesting an inclination angle of $\sim$75° if the ring is intrinsically circular. Last, the large line-of-sight optical depth required to hide warmer dust close to the young stellar objects is most easily explained by an edge-on disk model (see § 5). Thus, it is quite likely that the system has an inclination of $\geq$60°, placing the dynamical mass at 1.1–1.3 $M_\odot$.

Comparing the 1 $M_\odot$ mass derived for the gas and dust with the total system mass derived above clearly implies subsolar masses for the two central stellar cores. Yet the observed luminosity of 30–40 $L_\odot$ is larger than that expected from either solar mass main-sequence stars or pre–main-sequence objects. Theoretical tracks for pre–main-sequence objects in a purely convective phase of evolution (e.g., Stahler 1983) imply that the maximum luminosity attained by a 0.5–1 $M_\odot$ object is only 2–6 $L_\odot$. On the other hand, the luminosity could be produced purely by accretion onto the central objects; the total luminosity requires a total mass accretion rate of roughly 1×10^{-5} $(0.3\ M_\odot/M_c)(R_c/3\ R_\odot)\ M_\odot\ \mathrm{yr}^{-1}$, where M_c is the total mass in central objects and R_c is the radius of a central object. This accretion rate is considerably larger than corresponding rates in T Tauri stars of 10^{-7} to 10^{-8} $M_\odot$ yr^{-1} (e.g., Kenyon & Hartmann 1987) but similar to the rates predicted for spherical accretion in the Ophiuchus cloud (Adams, Lada, & Shu 1987, hereafter ALS). The time scale for consuming the observed circumstellar material, $\sim 10^5$ yr, is comparable to typical estimates for the lifetime of the embedded phase of pre–main-sequence evolution (Myers et al. 1987; Wilking, Lada, & Young 1989). Given that a substantial fraction of the system mass resides in circumstellar material and that the objects could still be accreting material from their surroundings, it appears the final stellar mass of the system will be close to the dynamical mass, i.e., $\sim 1\ M_\odot$.

5. MODELING THE CONTINUUM EMISSION

The spectral energy distribution (SED) of IRAS 16293−2422 is an extreme example of what is commonly observed from deeply embedded young stellar objects. The νS_ν energy distribution peaks beyond 100 μm wavelength; no emission has been detected at wavelengths shorter than 25 μm. The SED is well fitted with 40 K dust emission (Mundy et al. 1986) or with a combination of a 45 K compact source and a 20 K envelope (Mezger et al. 1990). This energy distribution is closest to that expected from a Class I object in the evolutionary sequence of ALS and Lada (1988), and the luminosity of IRAS 16293−2422 is consistent with their estimates for spherical accretion in Ophiuchus. However, the SED component expected from the near-infrared emitting protostellar core and warm inner disk is not seen. Moreover, the flattened region of NH_3 emission suggests that the gravitational influence of IRAS 16293−2422 may extend out to a radius of about 4000 AU, well beyond the expected free-fall region which lies at a radius of 2900 $(M/M_\odot)$ AU and also well beyond the radius where flattening is expected based on angular momentum considerations (ALS). It should be noted that the ALS models address the formation of a single star and the binary nature of IRAS 16293−2422 could contribute to the latter differences.

The lack of near-infrared emission is best explained by obscuration within the source itself. Observations presented here indicate that the millimeter dust emission arises from disks with maximum sizes of a few hundred AU. High-temperature dust must exist in the inner portions of such a disk. If the disk produces one-half of the observed flux at 100 μm, 500 Jy, then the fluxes at 12 and 25 μm would be 115 and 225 Jy, respectively, for a $T_{\mathrm{dust}} \propto r^{-0.5}$ law or 1220 and 925 Jy for a $T_{\mathrm{dust}} \propto r^{-0.75}$ law. For comparison, the color-corrected *IRAS* flux at 25 μm is 1.6 Jy and the upper limit to the *IRAS* flux at 12 μm is 0.07 Jy. Hence, this short-wavelength emission must be absorbed by intervening material with $\tau(25\ \mu\mathrm{m}) > 5$. The optical depth required to achieve $\tau = 1$ at 25 μm is roughly 4×10^{23} H_2 cm^{-2} (Hildebrand 1983; λ^{-1} emissivity). This column density is much larger than that in a hypothetical infall envelope supplying material at the accretion rate required to produce 30 $L_\odot$, $\sim 2 \times 10^{22}$ cm^{-2}; it is also much larger than the column density estimated for the extended cloud of 2–4 $\times 10^{22}$ cm^{-2} (Menten et al. 1987; Mundy et al. 1990). On the other hand, the column density through a 100 AU pathlength with an average density of 10^9 cm^{-3} is 3×10^{24} H_2 cm^{-2}. Therefore, it is most likely that the extinction occurs within the disk itself. If the disk is thick, and especially if it flares with increasing radius (e.g., Kenyon & Hartmann 1987), the inner hot dust could be obscured, over a range of viewing angles, by the outer, cooler portions of the disk. The observed SED is then characteristic of the outer disk plus the extended halo of material surrounding the source out to distances of thousands of AU.

6. SO ABUNDANCE VARIATIONS

As can be seen from Figure 1, the SO emission from IRAS 16293−2422 shows distinct differences from the 2.75 mm continuum emission. Since the observed SO transition (J, $K = 2$, 3–1, 2) arises from near the bottom of its J, K ladder and only 16 K above ground (see Gottlieb & Ball 1973 for an energy level diagram), the temperature and density throughout the continuum-emitting region is probably sufficient to ensure thermalized level populations. For example, the approximate critical density for the observed transition, using a collision rate constant characteristic of other diatomic molecules (5×10^{-11} cm^3 s^{-1}), is 10^6 cm^{-3}. Hence, differences between the observed SO and 2.75 mm emission distributions arise mainly from variations in the SO abundance.

The beam-averaged column density of SO can be calculated from the observations assuming thermalized level populations and a temperature for the gas. There are three characteristic temperatures for the region: 15–20 K from the large-scale NH_3 emission region, 40 K from the compact far-infrared emitting region, and 80 K derived from CH_3OH rotational diagrams (Blake, Grossbeck, & Phillips 1992). We will adopt 40 K but note that using 20 or 60 K results in a factor of 2 change in the column density. The SO column density is then given by

$$N(\mathrm{SO}) = \frac{3c^2}{16\pi^3\nu^3}\,\frac{Q(T)}{g_L}\,e^{E_U/kT}\,\frac{2J_L+1}{S(J_U, K_U - J_L, K_L)\mu^2}\,\frac{\int S_\nu\, dV}{\Omega_b},$$

where $Q(T)$ is the partition function, g_L is the degeneracy of the lower state, E_U is the energy of the upper state, $S(J_U, K_U - J_L, K_L)$ is the line strength as defined by Tiemann (1974), μ is the

dipole moment (1.55 debye; Tiemann 1974), and Ω_b is the beam solid angle. Expressed in convenient units,

$$N(\mathrm{SO}) = 1.7 \times 10^{14} \int S_\nu(\mathrm{Jy\ beam^{-1}}) dV(\mathrm{km\ s^{-1}}) \times \left(\frac{6''}{\mathrm{FWHM}}\right)^2 \mathrm{cm^{-2}}$$

for the observed transition. SO column densities corresponding to the contour levels in Figure 1*b* range from 3 to 30×10^{14} cm^{-2}. The uncertainty in these values is a factor of 2–3, mainly due to uncertainties in the kinetic temperature and molecular excitation.

A rough estimate of the fractional abundance of SO relative to H_2, X(SO), can be obtained from comparison with the 2.75 mm continuum map. Assuming the conversion relation, $N(H_2) = 6.6 \times 10^{25} \tau_{2.75\ \mathrm{mm}}$, X(SO) is 1.5×10^{-9} toward MM 1 and the upper limit toward MM 2 is 1.4×10^{-10}. Lower limits to the SO abundance toward the other emission clumps are around 2×10^{-9}. For comparison, measurement of the TMC-1 molecular cloud gives a value of 5×10^{-9} (Freeman & Millar 1983) and an estimate for the ρ Oph A core based on SO data (Gottlieb et al. 1978) and $C^{18}O$ data (Wilking & Lada 1983) yields $X(\mathrm{SO}) = 3 \times 10^{-9}$. Thus, within our stated uncertainties, the abundance of SO in MM 1 and associated SO clumps is consistent with that observed in dark cloud cores.

Variations in SO abundance, especially enhancements, have often been associated with shock activity (Hartquist, Oppenheimer, & Dalgarno 1980; Prasad & Huntress 1982; Mitchell 1984). For instance, the enhanced SO abundance in the plateau gas of Orion IRc2, 5×10^{-7}, relative to the extended ridge, $< 9 \times 10^{-10}$ (Blake et al. 1987), has been attributed to a high-temperature, oxygen-rich environment in a postshock gas (Prasad & Huntress 1982; Blake et al. 1987). Chemical models by Mitchell (1984) suggest that the SO abundance is most enhanced for shock speeds of 5–10 km s^{-1}. Interestingly, the SO abundance in MM 1, the active outflow source, appears to be relatively normal for dark cloud cores raising the point that MM 2 may be depleted in SO. Such a depletion could be the result of accretion of SO onto grains or chemical destruction. However, there is a factor of 3–4 uncertainty in all values of X(SO), hence the absolute sense of enhancement or depletion is much less certain than the relative variation in fractional abundance between MM 1 and MM 2.

The morphology of the SO emission and its peak at MM 1 suggest a relationship with the outflow activity indicated by the centimeter wavelength continuum and H_2O maser emission. The spatial distribution and velocity structure of the weaker SO emission to the east and west of MM 1 is reminiscent of the distribution of HCO^+ emission seen toward the HH 7–11 complex (Rudolph & Welch 1988). In both cases, the molecular gas shares aspects of the morphology of the outflow yet is detected at relatively low velocities, within a few km s^{-1} of line center. Based on 11″ resolution maps of the CS $J = 2$–1 transition toward IRAS 16293−2422, Walker et al. (1990b) suggest that the CS emission at 1.5–5 km s^{-1} from line center traces dense shells of ambient cloud material swept-up by the stellar wind. We propose that the extended SO emission traces regions of mild interaction between the outflow and ambient cloud where either the column density or fractional abundance of SO is enhanced, or some combination of the two. Detailed comparison between the CS and SO emission is difficult due to the difference in resolution. The velocity sense of the SO emission is opposite that of the large-scale CO outflow, but that comparison is also difficult because the velocity interval covered by the SO is mostly within the ambient cloud CO line.

7. SUMMARY

Since its discovery by *IRAS*, the far-infrared source 16293−2422 has been recognized as a young stellar object in the early phase of its evolution. Based on the high-resolution $\lambda = 2.75$ mm and centimeter wavelength continuum maps presented here, it appears that IRAS 16293−2422 is composed of two distinct sources with a projected separation of only 5″.2 or 840 AU. The southeastern source MM 1 contains $\sim 0.6\ M_\odot$ of gas and dust (assuming a dust emissivity law of λ^{-1}) within a 600×400 AU region. Its associated centimeter continuum emission is most likely produced by an ionized stellar wind as suggested by Wootten (1989). The northwestern source MM 2 displays continuum emission which increases as ν^2 through centimeter wavelengths and up to 2.75 mm. This unique spectrum can be explained if most of the millimeter wavelength emission arises from dust while the centimeter continuum emission derives from an optically thick H II region although it can not be ruled out that some or all of the centimeter emission arises from the warm inner regions of a disk. Assuming the 2.75 mm emission is from optically thin dust, MM 2 contains ~ 0.4 $M_\odot$ of gas and dust within a ≤ 400 AU diameter region. Given the compactness and mass of the circumstellar gas and dust, it is likely that the material is distributed in disks around the individual objects.

Walker et al. (1986) suggested that IRAS 16293−2422 was a collapsing protostar based on modeling of CS emission lines. While subsequent studies have shown this interpretation to be complicated by both rotational and outflow motions of the gas (e.g., Menten et al. 1987), our observations suggest that accretion is ongoing in this system. The combination of small projected separation, similarity of evolutionary state, and modest velocity shift between MM 1 and MM 2 suggest that they are in physical proximity within the cloud and probably represent a forming wide binary system. Extension of the NH_3 emission along the position angle of the proposed binary system provides further evidence for their association. Assuming the NH_3 probes the gravitational potential of the binary, a total dynamical mass of 1.1–1.3 $M_\odot$ is derived for the system; the distribution of this mass among stellar and circumstellar components suggests that the individual stellar masses are ≤ 0.5 $M_\odot$. Within current stellar models, such masses can only produce the observed 30–40 $L_\odot$ through accretion; an accretion rate of $\sim 10^{-5}\ M_\odot\ \mathrm{yr^{-1}}$ is implied, similar to that predicted by ALS. At that rate, the observed circumstellar material will be consumed in $\sim 10^5$ yr if there is no further infall.

From the morphology of the 1.3 cm emission, the spectral index of the centimeter wavelength emission and the presence of H_2O masers, it is evident that MM 1 is an active outflow source. Maps of the SO $J = 2$, 3–1, 2 transition show that the main SO emission is spatially coincident with MM 1. Weak additional emission was detected to the east and west of MM 1, but no emission was detected from MM 2. The SO abundance in the emission regions is estimated to be $\sim 2 \times 10^{-9}$, which consistent with larger scale estimates for ρ Oph A and other dark clouds, although this absolute abundance is uncertain by

a factor of 3–4. Nondetection of SO toward MM 2 requires its SO abundance to be down by a factor of 10 from MM 1. This may represent a real underabundance of gas-phase SO caused by depletion of SO into grain surfaces. We propose that the SO emission around MM 1 is enhanced relative to MM 2 due to the outflow activity and that the extended SO emission traces regions of mild interaction between the outflow and the ambient cloud.

We would like to thank the Owens Valley staff for their assistance in the observations. We thank Karl Menten and Doug Wood for helpful discussions and the referee for helpful comments. B. A. W. would like to thank C. J. Lada and J. M. Moran for their generosity during his visit at CfA. G. A. B. would like to acknowledge support from the Packard and Sloan Foundations. The OVRO millimeter interferometer is supported by NSF grant AST 87-14405 to Caltech.

REFERENCES

Abt, H. A., Gomez, A. E., & Levy, S. G. 1990, ApJS, 74, 551
Adams, F. C., Lada, C. J., & Shu, F. H. 1987, ApJ, 312, 788 (ALS)
André, Ph., Montmerle, T., Feigelson, E., & Steppe, H. 1990, A&A, 240, 321
Barsony, M., Burton, M. G., Russell, A. P. G., Carlstrom, J. E., & Garden, R. 1989, ApJ, 346, L93
Beckwith, S. V. W., Sargent, A. I., Chini, R. S., & Gusten, R. 1990, AJ, 99, 924
Blake, G. A., Grossbeck, T., & Phillips, T. G. 1992, in preparation
Blake, G. A., Sutton, E. C., Masson, C. R., & Phillips, T. G. 1987, ApJ, 315, 621
Butner, H. M., Evans, N. J., II, Lester, D. F., Harvey, P. M., Mundy, L. G., and Campbell, M. F. 1992, in preparation
Cabrit, S., & Bertout, C. 1986, ApJ, 307, 313
Chelli, A., Zinnecker, H., Carrasco, L., Cruz-Gonzales, I., & Perrier, C. 1988, A&A, 207, 46
Chen, W. P., Simon, M., Longmore, A. J., Howell, R. R., & Benson, J. A. 1990, ApJ, 357, 224
Duquennoy, A., & Mayor, M. 1990, in Proc. of the XI European Regional Astronomy Meeting, ed. M. Vasquez (Cambridge: Cambridge Univ. Press), in press
Edelson, R. A. 1987, AJ, 94, 1150
Estalella, R., Anglada, G., Rodríguez, L. F., & Garay, G. 1991, ApJ, 371, 626
Fomalont, E. B., Kellermann, K. I., Wall, J. V., & Weistrop, D. 1984, Science, 225, 23
Freeman, A., & Millar, T. J. 1983, Nature, 301, 402
Gottlieb, C. A., & Ball, J. A. 1973, ApJ, 184, L59
Gottlieb, C. A., Gottlieb, E. W., Litvak, M. M., Ball, J. A., & Penfield, H. 1978, ApJ, 219, 77
Hartquist, T. W., Oppenheimer, M., & Dalgarno, A. 1980, ApJ, 236, 182
Hildebrand, R. H. 1983, QJRAS, 24, 267
Kenyon, S. J., & Hartmann, L. 1987, ApJ, 323, 714
Lada, C. J. 1988, in Formation and Evolution of Low Mass Stars, ed. A. K. Dupree & M. T. V. T. Lago (Dordrecht: Reidel), 93
Lada, E. A., DePoy, D. L., Evans, N. J., & Gatley, I. 1991, ApJ, 374, 533
Maslowski, J., Pauliny-Toth, I. I. K., Witzel, A., & Kühr, H. 1984, A&A, 139, 85
McCaughrean, M. J., Zinnecker, H., Aspin, C., & McLean, I. S. 1991, in Astrophysics with Infrared Arrays, ed. R. Elston (NOAO: Tucson), 238
Menten, K. M., Serabyn, E., Gusten, R., & Wilson, T. L. 1987, A&A, 177, L57
Mezger, P. G., Sievers, A., & Zylka, R. 1990, in Fragmentation of Molecular Clouds and Star Formation, ed. E. Falgarone, F. Boulanger, & G. Duvert (Dordrecht: Reidel), 245
Mitchell, G. F. 1984, ApJ, 287, 665
Mizuno, A., Fukui, Y., Iwata, T., Nosawa, S., & Takano, T. 1990, ApJ, 356, 184
Mundy, L. G., Wilking, B. A., & Myers, S. T. 1986, ApJ, 311, L75
Mundy, L. G., Wootten, H. A., & Wilking, B. A. 1990, ApJ, 352, 159
Myers, P. C., Fuller, G. A., Mathieu, R. D., Beichman, C. A., Benson, P. J., Schild, R. E., & Emerson, J. P. 1987, ApJ, 319, 340
Prasad, S. S., & Huntress, W. T. 1982, ApJ, 260, 590
Rieke, G. H., Ashok, N. M., & Boyle, R. P. 1989, ApJ, 339, L71
Rudolph, A., & Welch, W. J. 1988, ApJ, 326, L31
Shu, F. H., Adams, F. C., & Lizano, S. 1987, ARA&A, 25, 23
Simon, M., Howell, R. R., Longmore, A. J., Wilking, B. A., Peterson, D. M., & Chen W. P. 1987, ApJ, 320, 344
Stahler, S. W. 1983, ApJ, 274, 822
Tiemann, E. 1974, J. Phys. Chem. Ref. Data, 3, 259
Walker, C. K., Adams, F. C., & Lada, C. J. 1990a, ApJ, 349, 515
Walker, C. K., Carlstrom, J. E., Bieging, J. H., Lada, C. J., & Young, E. T. 1990b, ApJ, 364, 173
Walker, C. K., Lada, C. J., Young, E. T., Maloney, P. R., & Wilking, B. A. 1986, ApJ, 309, L47
Walker, C. K., Lada, C. J., Young, E. T., & Margulis, M. 1988, ApJ, 332, 335
Weintraub, D., Sandell, G., & Duncan, W. 1989, ApJ, 340, L69
Wilking, B. A., & Claussen, M. J. 1987, ApJ, 320, L133
Wilking, B. A., & Lada, C. J. 1983, ApJ, 274, 698
Wilking, B. A., Lada, C. J., & Young, E. T. 1989, ApJ, 340, 823
Wood, D. O., & Churchwell, E. 1989, ApJS, 69, 831
Woody, D. P., Scott, S. L., Scoville, N. Z., Mundy, L. G., Sargent, A. I., Padin, S., Tinney, C. G., & Wilson, C. D. 1989, ApJ, 337, L41
Wootten, H. A. 1989, ApJ, 337, 858
———. 1992, in preparation
Wootten, H. A., & Loren, R. B. 1987, ApJ, 317, 220
Zinnecker, H., Perrier, C., & Chelli, A. 1988, in High-Resolution Imaging by Interferometry, ed. F. Merkle (Garching: ESO), 505